ELSEVIER

Diamond and Related Materials 11 (2002) 922–926

DIAMOND AND RELATED MATERIALS

www.elsevier.com/locate/diamond

Growth mechanism and properties of the large area well-aligned carbon nano-structures deposited by microwave plasma electron cyclotron resonance chemical vapor deposition

Chao Hsun Lin*, Hui Lin Chang, Ming Her Tsai, Cheng Tzu Kuo

Department of Materials Science and Engineering, National Chiao Tung University, Hsinchu 300, Taiwan, ROC

Abstract

Large area (4-inch diameter) well-aligned carbon nano-structures on Si substrate were successfully synthesized by using a catalyst-assisted microwave plasma electron cyclotron resonance chemical vapor deposition (ECR-CVD) system with CH_4 as source gas. The catalysts include Fe, Co and Ni. The catalysts and the deposited nano-structures were characterized by scanning electron microscopy (SEM), transmission electron microscopy (TEM), Raman and field emission *I–V* measurements. Effects of process parameters on morphologies, structures and properties of the nano-structures were examined. The results show that the deposited nano-structures can include normal nano-tubes, split catalyst nano-tubes, seaweed-like nano-sheets and carbon film, depending mainly on substrate temperature and bias, catalyst materials and their application methods. Deposition mechanisms for different nano-structures, especially, the unique split catalyst nano-tubes and seaweed-like nano-sheets, were proposed. The differences in oxidation resistance and field emission properties between different nano-structures will be compared and discussed.

Keywords: Carbon; Electron cyclotron resonance (ECR); Chemical vapor deposition (CVD); Catalytic processes

1. Introduction

Since the discovery of fullerenes in 1985 [1] and carbon nano-tubes (CNTs) in 1991 [2], materials science research and technology development on nano-structures have been intensively conducted in the world. The nano-structure materials have been synthesized from atoms and molecules of themselves, namely, self-assembly, to become nano-scaled nano-particles, nano-tubes, nano-wires, nano-layers, etc. They possess many special magnetic, electrical, physical or chemical properties as compared with the bulk materials. Therefore, the nano-structures have high potential applications in areas of dispersions and coating, high surface area materials, functional nano-devices, etc. [3].

Carbon nano-structures have been synthesized by a variety of methods, e.g. arc discharge [4], laser ablation [1], microwave plasma chemical vapor deposition (MPCVD) [5], template-based CVD [6], etc. A few deposition mechanisms for nano-structures have been proposed [7–9]. However, large area (>4 inch in diameter) carbon nano-tubes have not been successfully synthesized so far in the literatures, and the proposed deposition mechanisms could not successfully explain the formation of many different nano-sturctures. The purpose of this work was to synthesize various carbon nano-stuctures and to study their properties and formation mechanisms, and to develop large area deposition techniques for potential mass production researches in the future. It is known that the microwave plasma ECR-CVD has the advantages of high dissociation percentage of the precursor gas and high uniformity of plasma energy distribution, and was generally used for large area dry etching, surface cleaning, or diamond film deposition. Therefore, we adopted the advantages of ECR-CVD to synthesize large area carbon nano-structures without using templates, though ECR-CVD was used to synthesize CNTs or carbon nitride nano-tubes with anodic alumina as templates [10,11]

*Corresponding author. Tel.: +886-3-573-1949; fax: +886-3-572-1065.

E-mail address: ctkuo@cc.nctu.edu.tw (C.H. Lin).

0925-9635/02/$ - see front matter
PII: S0925-9635(01)00640-9

2. Experimental

Large area (4-inch diameter) well-aligned CNTs were synthesized on Si wafer by using catalyst-assisted ECR-CVD method with CH_4 as gas source. The transition metals acted as catalysts include Fe, Ni and Co metals. The Fe, Co and Ni catalysts were applied on the substrate surfaces by spin coating a thin layer of iron nitrate $[Fe(NO_3)_2]$, cobalt nitrate $[Co(NO_3)_2]$, or nickel acetate $[Ni(OOCCH_3)_2]$ in 1 M water solutions, respectively. Then the spin-coated substrates were dried in air and reduced in 10-sccm flow rate of hydrogen plasma at approximately 600 °C substrate temperature for 15 min to become well-distributed nano-sized catalysts. The catalyst-coated substrates were then deposited with nano-structures in the same ECR-CVD system under 875-Gauss magnetic field strength by varying different deposition conditions. The substrate temperatures were varied by a substrate heater and plasma heating effect from 330 to 600 °C. The substrates were subjected to either 0 V or −100 V bias. The deposited nano-structures were characterized by FESEM (field emission scanning electron microscopy), TEM, HRTEM (high resolution transmission electron microscopy), Raman spectroscopy and I–V measurements. The TEM specimens were prepared by immersing and agitating the specimens in an ultrasonic acetone bath to disperse the nano-structures. Then the droplets with the dispersed nano-structures were dropped and dried on a carbon-coated Cu mesh for TEM examination.

3. Results and discussion

3.1. Effect of catalyst types on carbon nano-structure growth

The growth mechanisms for CNTs and nano-sheets were examined by comparing different catalytic-grown nano-structures. The SEM micrographs for the Fe, Co and Ni catalyst-coated substrate surfaces and the Si substrate itself, before nano-structure depositions, are shown in Fig. 1a–d. The corresponding as-deposited nano-structures are depicted in Fig. 1e–h, respectively, under the same deposition conditions (20 sccm CH_4, 800 W microwave power, 600 °C substrate temperature, −100 V substrate bias, and 15 min deposition time). These figures indicate that either the Fe catalyst or no catalyst applications show nano-sheet-like nano-structures and have no nano-tube formation (Fig. 1e,h). The Fe catalyst particles in Fig. 1a are approximately 30∼45 nm in size, but the particles with relative shallow boundaries are embedded tightly like a film. This may relate to a higher sintering effect of Fe particles than other catalysts under the same catalyst reduction process at 600 °C. In other words, the tightly sintered particles will be more difficult to melt during deposition to become nano-scaled liquid droplets, which are pushed upward individually to form nano-tubes, according to the catalyst-assisted nano-tube tip-growth mechanism [7]. The same reasoning can be applied to the case of no catalyst applications in Fig. 1h. In these cases of the nano-sheet formation, the C_2 (C–C bond) bonds in the initial stage from the precipitated carbons and/or free carbons may form nucleus structures and be connected linearly with each other on the surface of the tightly sintered catalyst particles or the substrate without catalyst applications. The free carbons from the plasma atmosphere will further adhere on the existing structure to become a scale-like carbon sheet. The sheets are then connected with each other in wavy fashion to become seaweed-like nano-sheets. In an ECR plasma system with the substrate bias, the gas dissociation is mainly controlled by microwave power with assistance of ECR. The kinetic energy of positive ions is mainly manipulated by the negative substrate bias [12]. Furthermore, since the ECR-CVD system is working under lower pressure (2×10^{-3} torr), most of the ion motion trajec-

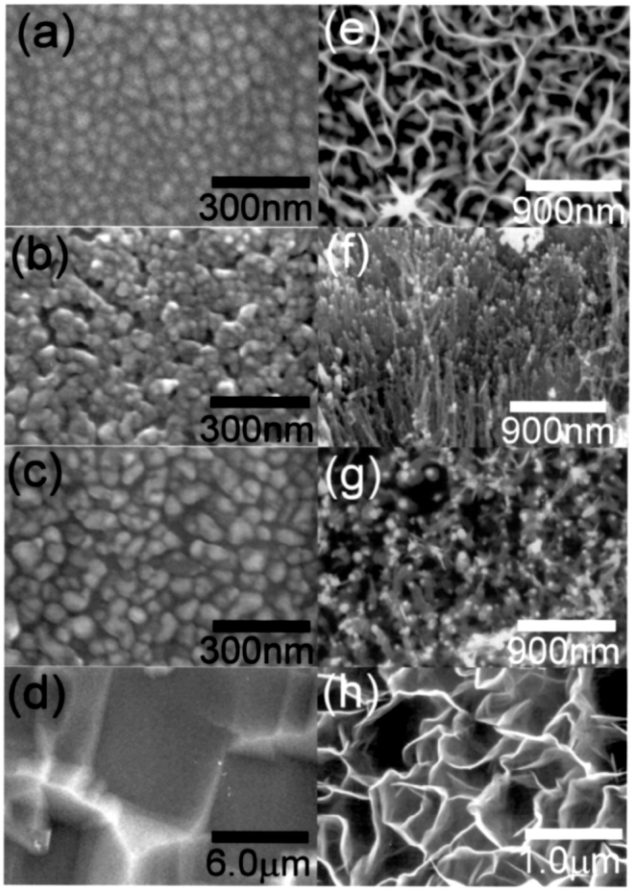

Fig. 1. SEM micrographs of catalysts: (a) Fe catalyst; (b) Co catalyst; (c) Ni catalyst and (d) Si substrate. The corresponding as-deposited nano-structures: (e) Fe catalytic grown nano-sheets; (f) Co catalytic grown CNTs; (g) Ni catalytic grown CNTs and (h) the nano-sheets on Si substrate without catalyst application.

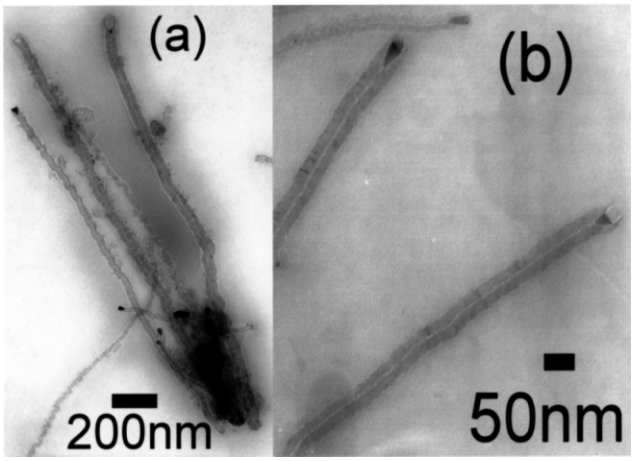

Fig. 2. TEM micrographs: (a) Co and (b) Ni catalytic grown CNTs.

tory will be vertical to the substrates. Therefore, the nano-sheets (approx. 20 nm in thickness) are perpendicular to the substrate surface.

The factors to determine the CNT morphologies were studied by examining the differences in the Co and Ni catalytic-grown CNTs in Fig. 1f,g, which are corresponding to the side view and top view of the tubes, respectively. It is noted that the sizes of the Co catalyst particles in Fig. 1b are ranging from 30 nm to 80 nm, which are approximately the sizes of the nano-tubes in Fig. 1f. The same conclusion is applied to the Ni catalytic grown CNTs in Fig. 1g, where the tube diameters are in the range of 30–60 nm. This is in agreement with the reported statement that the sizes of the catalyst particles determine the diameters of the nano-tubes [8–10]. As to the tube-number densities, a smaller particle size combining with a denser distribution of the catalyst particles on the substrate surface can result in a higher tube-number density. Under the present deposition conditions, the tube-number densities of the CNTs for Ni catalyst ($55\sim60\times10^6$ tubes/cm^2) are greater than for Co catalyst ($30\sim35\times10^6$ tubes/cm^2). Regarding the shapes of the tubes, Fig. 2a,b reveals the TEM micrographs of Co and Ni catalytic grown CNTs. From Fig. 2, the catalysts at the tube caps are obvious, though some of the catalysts are missing due to TEM sample preparation. This implies that the growth mechanism in these cases is the tip growth mechanism [7]. The Co catalytic grown CNT tip lattice image by HRTEM around a catalyst particle is shown in Fig. 3. It shows that the catalyst cap conforms closely to the nano-tube core and the multiple graphene layers are 0.34 nm in spacing, which is in agreement with the reported value for CNT wall spacing [13].

3.2. Growth mechanism of the split catalyst nano-tubes

According to the tip growth mechanism, the catalyst is pushed upward by the growing nano-tubes, and the whole catalyst particle becomes the cap of the tubes. It is interesting to note that the Co catalysts are not only located at the caps of the tubes but also separately at few sites along the center of the tubes, as shown in Fig. 4. This may be reasoned by imagining the Co catalyst is split into few small pieces following a bigger mother catalyst at the tube cap. These types of nano-tubes will be called the 'split catalyst nano-tubes'. They are more often found in the bigger catalysts or tubes. Regarding the splitting action, the capillary force from the tube center hole and the known gravity force of the catalyst will most probably elongate the liquid drop of the larger catalyst particle into the tube center during the tube growth. The tube growth direction may also most probably be altered for a larger catalyst, because it is similar to an unstable one-dimension structure with overweight at one end. Furthermore, the change in growth direction will most probably cause the splitting of the elongated liquid drops. The split droplets will be left on the original sites by the capillary force. This is supported by the fact that the split positions are often at locations where the tube changes the growth direction.

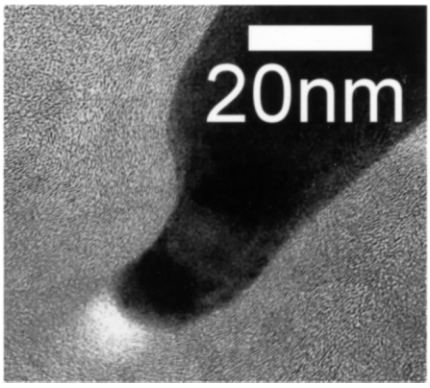

Fig. 3. HRTEM micrograph of CNT lattice image around Co catalyst particle.

3.3. Effects of other process parameters on carbon nano-structure formation

Besides catalyst type, particle size and shape, the nano-structures are also strongly affected by substrate temperature and bias. The results show that the required conditions to form three different nano-structures (nano-tubes, seaweed-like nano-sheets and carbon films) are

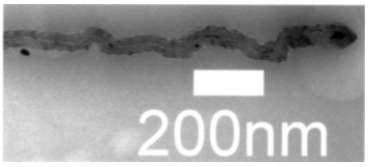

Fig. 4. TEM micrograph of the 'split Co catalyst nano-tubes'.

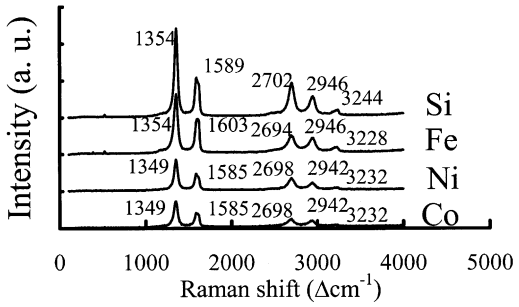

Fig. 5. Raman spectra of the Co and Ni catalytic grown CNTs, the Fe catalytic grown nano-sheets, and the nano-sheets on Si substrate with no catalyst application, respectively (deposition time 15 min, 20 sccm CH_4).

as follows. For nano-tube formations, the required conditions include higher substrate temperature (>560 °C), negative substrate bias and catalyst application. As to seaweed-like nano-sheets formation, the required conditions are the same as the nano-tubes except without the catalyst application. However, the carbon film will form if the substrate temperature is not high enough. It is obvious that both the substrate temperature and bias are necessary conditions to form nano-tubes and seaweed-like nano-sheets. It is believed that the effect of substrate temperature is to minimize the thermal energy required to activate the catalysts to precipitate carbon atoms to form nano-tubes or to activate the substrate surface to accommodate carbon atoms to form carbon nano-sheets. Moreover, effect of the negative substrate bias is to attract and accelerate the positive species in plasma to stick into and form the nano-structures. The unique feature of the well-aligned nano-tubes and nano-sheets perpendicular to the substrate surfaces may be a consequence of the substrate bias effect plus the action of magnetic field to generate ECR condition, as discussed in the previous paragraph.

3.4. Raman spectra of the nano-structures

Fig. 5 is the micro-Raman spectra of the different catalytic growth nano-structures on Si substrate. The excitation laser is a 514.5-nm Ar-ion laser. The D-line, 2nd order D-line and D′-line are from 1349–1354 cm^{-1}, 2694–2702 cm^{-1} and 3228–3244 cm^{-1}, respectively. The corresponding G-line and the combination of D- and G-line are from 1585–1603 cm^{-1} and 2942–2946 cm^{-1}, respectively. Here, the Fe catalytic and non-catalytic grown nano-sheets have relatively higher wave numbers of D- and G-line than in the Ni and Co catalytic grown multi-walled nano-tubes. According to Cooper and Young [14], the tensile stress in the nano-tubes can cause Raman peak positions shifting to a lower wave number side. This may imply that the nano-tubes suffer a tensile residual stress by comparing with that in the nano-sheets, because the nano-sheets can be considered to consist of the graphene planes without bending stress. It can be reasoned by the fact that bending the graphene planes to a tube shape forms the nano-tubes. This is supported by the fact that the wave numbers of the Raman peaks for SWNTs (single-walled nano-tubes) are generally lower than that for MWNTs (multi-walled nano-tubes) due to a greater bending or higher tensile residual stress in SWNTs. The reported D-line and G-line peaks for nano-tubes are approximately 1308–1349 cm^{-1} and 1532–1594 cm^{-1}, respectively [14–17]. In other words, the D-line (1349 cm^{-1}) and G-line (1585 cm^{-1}) peak positions of our nano-tubes are closer to the higher wave number side. This means that our nano-tubes suffer a less tensile stress than the reported nano-tubes from the literatures.

Regarding $I(G)/I(D)$ ratio, the ratios for the Ni and Co catalytic grown nano-tubes are 0.55 and 0.57, respectively. In contrast, the ratios for Fe catalytic grown and no catalytic grown nano-sheets are 0.59 and 0.45, respectively. This implies that the catalytic grown nano-tubes or nano-sheets possess more G–bonding than non-catalytic grown nano-sheets. In other words, the catalysts can enhance the G–bond formation in addition to assisting the tube formation.

3.5. Oxidation resistance of the nano-structures

Oxidation resistance of carbon nano-tubes was examined under air atmospheres at 300–600 for 30 min. The Co catalytic grown nano-tubes are purified in structure at 300 °C, collapsed at 450 °C, and burned at 600 °C. In contrast, the Ni catalytic grown nano-tubes are purified without structure collapse up to 450 °C, and also burned at 600 °C. In other words, the oxidation resistance of the Ni catalytic-grown nano-tubes is greater than the Co catalytic grown nano-tubes. This may imply that the Co catalytic grown nano-tubes contain more structure defects. This is supported by TEM examination in Fig. 2a,b.

3.6. Field emission properties of the nano-tubes

The $I–V$ curves of the 5th cycle test to represent the field emission properties of the relatively stable state of the nano-structures are shown in Fig. 6. It indicates that the Co catalytic grown nano-tubes possess the best properties with current density beyond the instrument capability. The results also show that the emission properties depend on the catalyst type. The order in magnitude of emission current density of the nano-structures for various catalyst applications is Co (>32 mA/cm^2) >Ni (19.8 mA/cm^2) >Fe (7.1 mA/cm^2) > no catalyst (2.5 mA/cm^2) at 10 V/μm. The turn-on voltages are in order of Ni (1.1 V/μm) <Co (3.0 V/μm) <no catalyst (4.6 V/μm) =Fe (4.6 V/μm). By

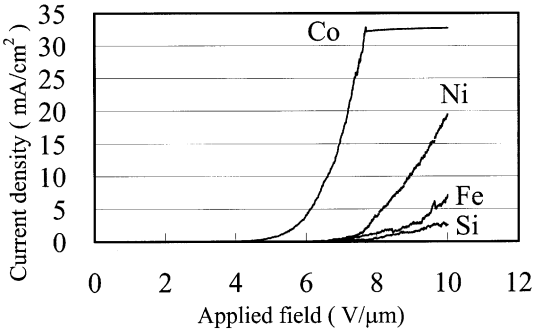

Fig. 6. Field emission I–V curves of the Co and Ni catalytic grown CNTs, the Fe catalytic grown nano-sheets, and the nano-sheets on Si substrate with no catalyst application, respectively (deposition time 15 min, 20 sccm CH_4).

comparing the Co and Ni catalytic grown nano-tubes, the better emission current density for the former one must relate to a combination effect of the tube morphologies. The Co catalytic grown nano-tubes possess a proper combination of tube diameter and tube-number density to minimize the screen effect among neighbor tubes to enhance the effective emission area, which may compensate insufficient in-field enhancement factor due to a lower aspect ratio of tube length-to-diameter. In other words, the best field emission properties can be improved by decreasing the tip radius of the tubes and manipulating a proper tube-number density. For Co catalytic grown nano-tubes, the current density can reach 32 mA/cm^2 at 7.6 $V/\mu m$; and the threshold voltage can go down to 6.6 $V/\mu m$.

4. Conclusions

The deposition conditions to synthesize different nano-structures, including normal CNTs, unique split catalyst CNTs and seaweed-like carbon nano-sheets, were examined. The catalyst types and their application methods, substrate temperature and bias are found to be the crucial parameters of determining the deposited nano-structures and their properties. The growth mechanisms for different nano-structures, especially 'split catalyst nano-tubes' and 'seaweed-like nano-sheets', were proposed. The relationships between the nano-structures and properties were studied. The properties of different catalytic grown nano-tubes were compared. The properties including Raman $I(G)/I(D)$ ratio, oxidation resistance and field emission were determined. The results show that the morphologies (i.e. tube length, diameter, shape and tube-number density) and the structure defects of CNTs depend on catalyst type and its application method. The CNTs with less structure defects may result in a higher oxidation resistance. This explains why the Ni catalytic grown nano-tubes have a better resistance than the Co catalytic grown tubes, As to field emission properties of the CNTs, the Co catalytic grown CNTs possess better properties (current density $=32$ mA/cm^2 at 7.6 $V/\mu m$, turn-on voltage $=3.0$ $V/\mu m$, threshold voltage $=6.6$ $V/\mu m$). The best field emission properties can be improved by decreasing the tip radius of the tubes and manipulating a proper tube-number density.

Acknowledgments

This work was supported by the National Science Council (contract no.: NSC89-2216-E-009-020 and-019), the Ministry of Education (contract no.: 89-E-FA06-l-4) and the ITRI-MRL of Taiwan (contract no. 90-3XS2542 or NCTU-C90098).

References

[1] H.W. Kroto, J.R. Heath, S.C. O'Brien, R.F. Curl, R.E. Smally, Nature 318 (1985) 162.
[2] S. Iijima, Nature 354 (1991) 56.
[3] R.W. Seigel, in: G.M. Holdridge (Ed.), Nano-structure Science and Technology, Kluwer Academic Publishers, Netherlands, 1999, pp. 1–13.
[4] T.W. Ebbesen, Carbon Nano-tubes Preparation and Properties, CRC Press, New York, 1997.
[5] T.A. Habermann. Gohl, K. Janischowsky, D. Nau, M. Stammler, L. Ley, G. Muller, in: Proc. 11th Intl. Microelectronics Conference, 1998, p. 200.
[6] A. Huczko, Appl. Phys. A 70 (4) (2000) 365.
[7] X.H. Chen, S.Q. Feng, Y. Ding, J.C. Peng, Z.Z. Chen, Thin Solid Films 339 (1999) 6.
[8] C.J. Lee, D.W. Kim, T.J. Lee, Y.C. Choi, Y.S. Park, Y.H. Lee, W.B. Choi, N.S. Lee, G.S. Park, J.M. Kim, Chem. Phys. Lett. 312 (1999) 461.
[9] S.B. Sinnott, R. Andrews, D. Qian, A.M. Rao, Z. Mao, E.C. Dickey, F. Derbyshire, Chem. Phys. Lett. 315 (1999) 25.
[10] S.H. Tsai, F.K. Chiang, T.G. Tsai, F.S. Shieu, H.C. Shih, Thin Solid Film 366 (2000) 11.
[11] S.L. Sung, S.H. Tsai, C.H. Tseng, F.K. Chiang, X.W. Liu, H.C. Shih, Appl. Phys. Lett. 74 (2) (1999) 197.
[12] S.W. Pang, in: A.N. Goldstein (Ed.), Handbook of Nano-phase Materials, Marcel Dekker, New York, 1997, p. 15.
[13] P.M. Ajayan, in: H.S. Nalwa (Ed.), Handbook of Nano-structured Materials and Nano-technology, Academic Press, San Diego, 2000, p. 377.
[14] C.A. Cooper, R.J. Young, in: D. Tomanek, R.J. Enbody (Eds.), Science and Application of Nano-tubes, Kluwer Academic, New York, 2000, p. 93.
[15] S.J. Chung, H.S. Kim, J. Jang, S.H. Lim, C.H. Lee, B.Y. Moon, SID 01 DIGEST, Society of Information Display, San Jose, 2001, p. 92
[16] J.M. Kim, W.B. Choi, N.S. Lee, J.E. Jung, Diamond Relat. Mater. 9 (2000) 1184.
[17] R.R. Bacsa, Ch. Laurent, A. Peigney, W.S. Basca, Th. Vaugien, A. Rousset, Chem. Phys. Lett. 323 (2000) 566.